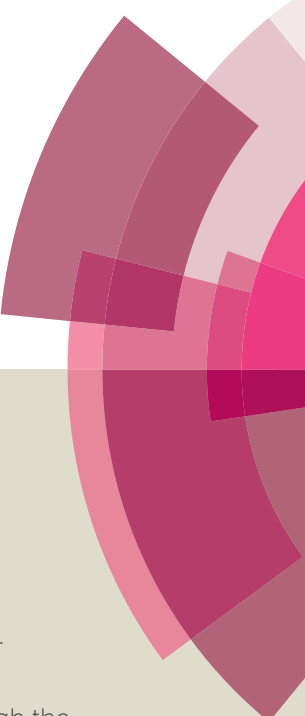
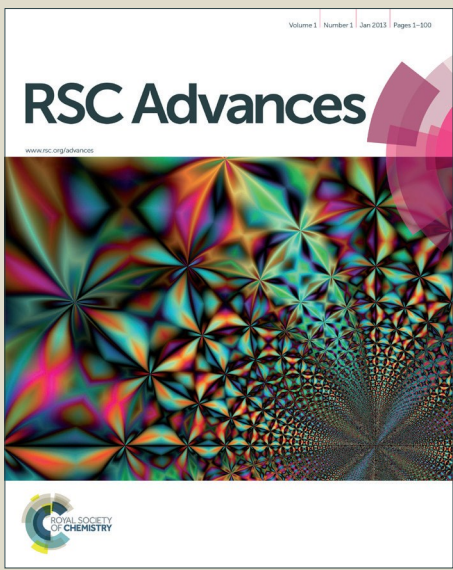


RSC Advances



This article can be cited before page numbers have been issued, to do this please use: A. A. Alhwaige, S. M. Alhassan, M. S. Katsiotis, H. Ishida and S. Qutubuddin, *RSC Adv.*, 2015, DOI: 10.1039/C5RA16188F.



This is an Accepted Manuscript, which has been through the Royal Society of Chemistry peer review process and has been accepted for publication.

Accepted Manuscripts are published online shortly after acceptance, before technical editing, formatting and proof reading. Using this free service, authors can make their results available to the community, in citable form, before we publish the edited article. This Accepted Manuscript will be replaced by the edited, formatted and paginated article as soon as this is available.

You can find more information about Accepted Manuscripts in the [Information for Authors](#).

Please note that technical editing may introduce minor changes to the text and/or graphics, which may alter content. The journal's standard [Terms & Conditions](#) and the [Ethical guidelines](#) still apply. In no event shall the Royal Society of Chemistry be held responsible for any errors or omissions in this Accepted Manuscript or any consequences arising from the use of any information it contains.

1 **Interactions, Morphology and Thermal Stability of Graphene-Oxide**
2 **Reinforced Polymer Aerogel Derived from Star-Like Telechelic Aldehyde-**
3 **Terminal Benzoxazine Resin**

4

5 **Almahdi A. Alhwaige^{1,2,*†}, Saeed M. Alhassan³, Marios S. Katsiotis³, Hatsuo Ishida^{2,*}, Syed**
6 **Qutubuddin^{1,2,*}**

7 *¹Department of Chemical and Biochemical Engineering, Case Western Reserve University,
8 Cleveland, Ohio 44106-7217, USA*

9 *²Department of Macromolecular Science and Engineering, Case Western Reserve University,
10 Cleveland, OH 44106-7202, USA*

11 *³Department of Chemical Engineering, The Petroleum Institute, United Arab Emirates*

12

13

14

15

16

17

18

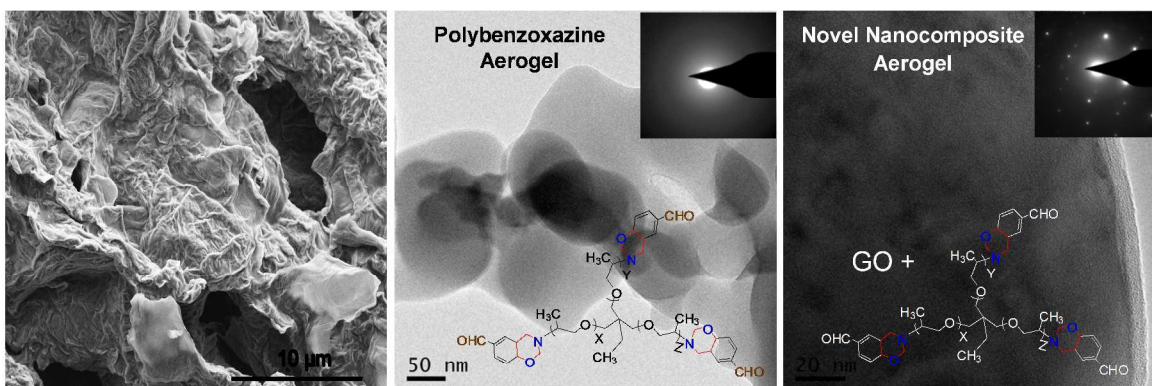
19

20

21 ^{*}Corresponding authors: aaa148@case.edu (Almahdi Alhwaige), sxq@case.edu (Syed
22 Qutubuddin), and hxi3@case.edu (Hatsuo Ishida).

23 [†]On leave from Al-Mergib University, Libya (aaalhwaige@elmergib.edu.ly).

1

2 **Table of Contents Entry**

3 Morphological properties of polybenzoxazine/graphene oxide aerogels

4

5

6

7

8

9

10

11

12

13

14

15

16

17

18

19

20

21

22

23

24

1 ABSTRACT

2 Graphene oxide (GO)-reinforced nanocomposite aerogels of polybenzoxazine prepared
3 via freeze-drying of GO suspensions in benzoxazine precursor solutions has been studied. The
4 synthesis of GO is confirmed using Raman and Fourier transform infrared (FT-IR) spectroscopy.
5 Benzoxazine monomer (SLTB(4HBA-t403)) has been synthesized using 4-hydroxybenzaldehyde
6 as a phenolic component, paraformaldehyde, and tri-functional polyetheramine (Jeffamine T-
7 403) as an amine source. The chemical structure of the benzoxazine monomer is confirmed by
8 nuclear magnetic resonance ($^1\text{H-NMR}$) spectroscopy and FT-IR. The interactions of GO and
9 SLTB(4HBA-t403) have been investigated using FT-IR. The morphological and thermal stability
10 of nanocomposite aerogels are examined and compared with the neat polybenzoxazine aerogel.
11 The structures of the aerogels and the effect of GO on the morphology of the aerogels are studied
12 using X-ray diffraction (XRD), scanning electron microscopy (SEM), and transmission electron
13 microscopy (TEM). The effect of GO on the ring-opening polymerization of benzoxazine is also
14 evaluated using differential scanning calorimetry (DSC) whereas the thermal stability of the
15 nanocomposite aerogels is characterized by thermogravimetric analysis (TGA).

16

17 **KEYWORDS:** *Graphene oxide, polybenzoxazines, nanocomposite aerogels, morphology, and*
18 *thermal properties.*

19

20

21

22

23

24

1. INTRODUCTION

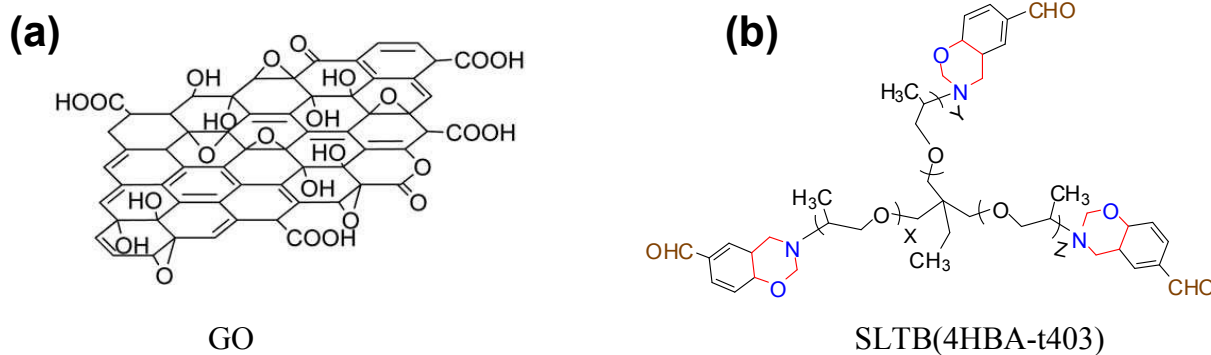
2 Aerogels are open-cell porous three-dimensional materials with unusual properties such as
3 ultralow density (0.05-0.1 g/cm³), high surface area, and low dielectric permittivity.¹⁻⁴ Since
4 Kistler¹ developed the aerogels in 1931, sol-gel process has attracted much attention for the
5 fabrication of porous materials.⁴ However, active research in this area did not start until about 40
6 years later.² The nano-porous open structure of aerogels, which are formed by replacing the
7 liquid in a gel with gas during their preparation and persists in the dry state.^{2,5,6} The efficiency of
8 cross-linking polymers is expected to produce aerogels with much better properties.²

9 Among the cross-linking polymers, polybenzoxazines have gained much attention as a
10 versatile class of attractive polymeric materials.⁷⁻¹¹ Although the first synthesis of small
11 molecular weight benzoxazine was reported in 1940s,¹² the synthesis and properties of
12 polybenzoxazine derived from monomeric type benzoxazine resins was reported in 1994.¹³ More
13 recently, main-chain type cross-linkable polybenzoxazines where the oxazine ring is placed in
14 the main chain have been developed.¹⁴ The development of polybenzoxazine aerogels was first
15 reported in 2009.¹⁵ Meanwhile, several other studies on polybenzoxazine-based polymeric and
16 carbon aerogels containing different monomers have been reported.^{6,7,16-20} The advantages of
17 benzoxazine-based nanostructured materials include near-zero shrinkage upon polymerization,
18 excellent thermal stability, and high char yields.^{17,21}

19 Nanocomposite materials are regarded one of the fastest growing fields in the polymer
20 industry.²² Specific properties of polymeric materials can be enhanced by a uniform dispersion of
21 reinforcement in the polymer matrix, in particular using a small quantity of nanofiller.²³⁻²⁷ Many
22 different types of fillers, including clay, carbon black, graphene, carbon nanotubes, carbon fibers,
23 and glass fibers have been investigated for producing materials with improved properties.

1 Growing literature about the still-developing field of polybenzoxazine nanocomposites presents
2 major advances that are worthy of consideration. Polybenzoxazine based nanocomposites have
3 attracted the interest of researchers in film form; however, research in development of
4 polybenzoxazine-based nanocomposite aerogels is limited. Very recently, graphene-reinforced
5 benzoxazine films have been investigated.²⁸⁻³⁰ The current study, involves the incorporation of
6 GO into aldehyde-terminal benzoxazine matrix in the form of nanocomposite aerogel, which has
7 not yet been reported.

8



11 **Scheme 1** Chemical structures of: (a) graphene oxide (GO) and (b) the star-like telechelic
12 benzoxazine monomer (SLTB(4HBA-t403)) used in this work.

13

14 Graphene nanosheets show unusual enhancement on the properties of nanocomposite
15 materials.³⁰⁻³² GO (Scheme 1a) is a layered material produced by the treatment of natural
16 graphite using strong mineral acids and effective oxidizing agents, which introduce a variety of
17 oxygen-based functional groups to the basal planes and edges of graphene layers.³¹⁻³⁷ Graphite is
18 the inexpensive natural source available for production of graphene and GO sheets.^{30-34,38}

19 Polymer composites with exfoliated graphite have been reported since 1958.³¹ The forces of
20 interaction between the polymers and GO are primarily dipole-dipole interaction and/or

1 hydrogen bonding arising from the polar groups in the polymer and covalent bond formation
2 with the functional groups of hydroxyl (-OH), epoxide (-COC-), and carboxyl (-COOH) on the
3 surfaces of the GO. For example, graphene-based nanocomposite studies were reported using
4 polymers, such as polybenzoxazine,^{29,30} polyaniline,³² polystyrene-polyacrylamide copolymer,³³
5 poly(allylamine),³⁹ poly(vinyl alcohol),⁴⁰ and epoxy.⁴¹ The development of carbon-based
6 aerogels from graphene and GO have been reported.^{42,43}

7 Combination of benzoxazine and GO is a promising approach to develop the field of
8 benzoxazine nanocomposite aerogels with properties not provided by neat polybenzoxazines. In
9 the current study, a star-like telechelic benzoxazine (Scheme 1b) was used with various GO
10 contents for synthesizing novel nanocomposite aerogels. The morphological and thermal stability
11 of these aerogels have been studied in detail. The novelty of the current study involves our report
12 on the first proposed mechanism of interaction between aldehydes-terminal benzoxazine and GO
13 nanosheets.

14

15 2. EXPERIMENTAL SECTION

16 2.1. Reagents

17 Graphene oxide (GO) was synthesized from natural graphite powder by modified Hummer's
18 method as previously described.^{44,45} Synthesis of GO is described in the Supporting Information,
19 S1.2. Graphite powder (micro 850) was obtained from Asbury Graphite Mills, Inc. Concentrated
20 sulfuric acid (H_2SO_4 , 98%), potassium permanganate ($KMnO_4$ crystal), hydrogen peroxide
21 (H_2O_2 , 30% aqueous solution), concentrated hydrochloric acid (HCl) were purchased from
22 Fisher Scientific (USA).

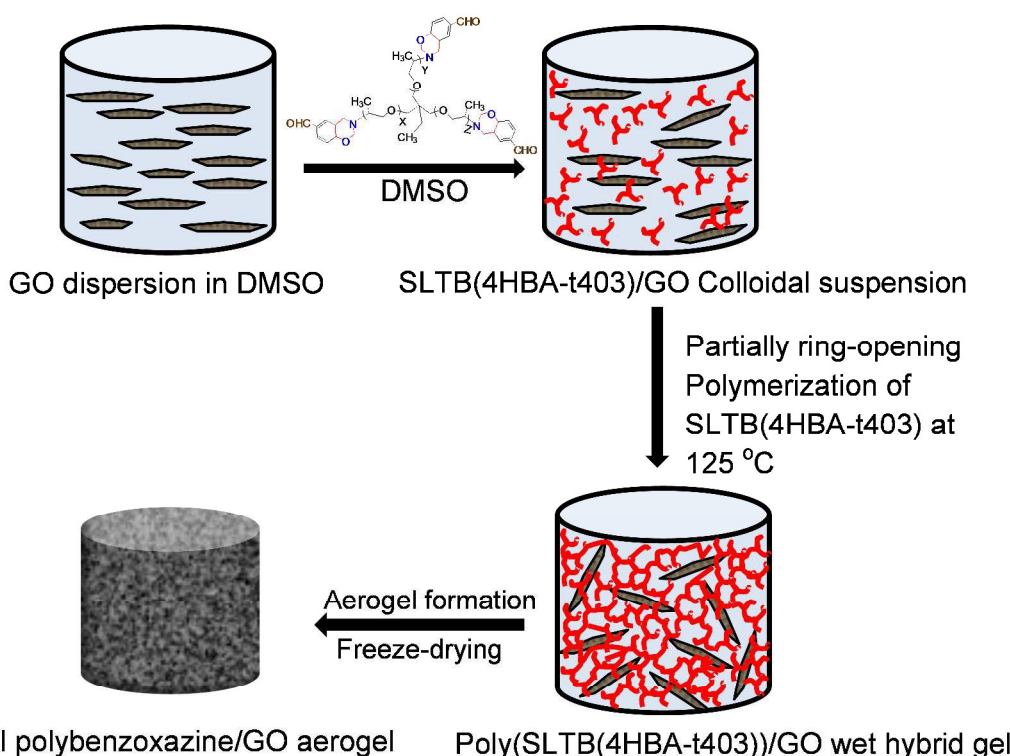
1 Star-like telechelic benzoxazine was synthesized from 4-hydroxybenzaldehyde (4HBA,
2 98%, Aldrich Chemicals, USA), polyetheramine (Star-like jeffamine T-403, Mn = 403 g/mol,
3 kindly supplied by Huntsman) and paraformaldehyde (96% w/w, Sigma-Aldrich Chemicals,
4 USA) using 1,4-dioxane as solvent. The telechelic is hereinafter abbreviated as SLTB(4HBA-
5 t403). Glacial acetic acid (CH_3COOH), 1,4-dioxane, chloroform, and dimethylsulfoxide (DMSO)
6 were purchased from Fisher Scientific (USA). All chemicals were used without further
7 purification.

8 **2.2. Preparation of SLTB(4HBA-t403)/GO nanocomposite aerogels**

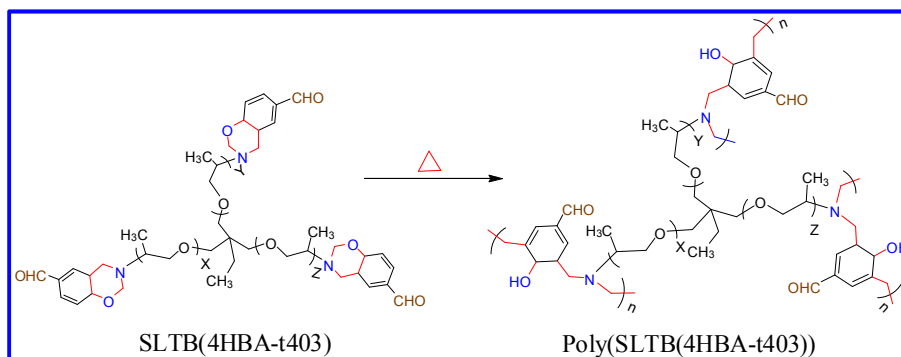
9 New nanocomposite aerogels were prepared via freeze-drying of various GO suspensions in
10 SLTB(4HBA-t403) solutions (Fig. 1). Samples are abbreviated as SLTB(4HBA-t403)/GO-
11 where x is the various GO content of 0, 3, 5, and 10 wt%. The starting precursor of benzoxazine
12 (SLTB(4HBA-t403)) was prepared by our previously reported method⁴⁶ and can be found in the
13 Supporting Information, S1.3. The preparation of the aerogels will be presented using
14 SLTB(4HBA-t403)/GO-5 as an example of nanocomposite aerogel containing 5 wt% GO.
15 Specifically, 0.05 g of GO were dispersed in 10 mL of DMSO, while at the same time, 0.95 g of
16 SLTB(4HBA-t403) were dissolved in 10 mL of DMSO using a magnetic stirrer at ambient
17 conditions. After completely dissolving SLTB(4HBA-t403), the solution was added slowly to the
18 GO colloidal suspension under vigorous agitation using a mechanical stirrer at 1000 rpm at room
19 temperature. The mixing lasted for 3 h, after which the mixture was sonicated for 30 min. Then,
20 the collected suspension was transferred into glass vials, sealed, and then heated slowly to 125
21 °C in an oven for 24 h. The attained nanocomposite product was partially cross-linked due to
22 ring-opening polymerization of benzoxazine precursor.¹⁵ The collected colloidal suspension was
23 frozen using ethanol and solid carbon dioxide at -70 °C and ambient pressure. Finally, the frozen

1 poly(4HBA-t403/GO- x) suspension was transferred to a VirTis AdVantage@ EL-85 freeze-drier
 2 for five days. Aerogels were obtained after drying the frozen solvent by sublimation under high
 3 vacuum conditions.

4



5
 6 **Fig. 1** Illustration of preparation process for novel polybenzoxazine/GO nanocomposite aerogels.
 7



8
 9 **Scheme 2** Thermally accelerated synthesis of poly(SLTB(4HBA-t403)) from its precursor.

1 2.3. Cross-linking and carbonization of the aerogels

2 The resulting aerogels were thermally treated at 150 °C, 175 °C, and 180 °C for 2 h to obtain the
3 fully polymerized and cross-linked polybenzoxazine nanocomposite aerogels (Scheme 2). The
4 polymerized aerogels were carbonized under nitrogen flow of 60 mL/min and a temperature
5 ramp rate of 10 °C/min from ambient temperature to 900 °C.

6 2.4. Characterization

7 Micro-Raman scattering studies were carried out at room temperature using a Horiba Jobin-Yvon
8 LabRam HR800 spectrometer which is equipped with a charge coupled detector and two grating
9 systems (600 and 1800 lines/mm). A HeNe laser ($\lambda = 632.8$ nm), with an optical power of 17
10 mW and a spot size of $1 \mu\text{m}^2$, was focused on the sample with an Olympus microscope. Raman
11 shifts were calibrated with a Si (100) wafer using the 520 cm^{-1} peak.

12 X-ray diffraction (XRD) was used to determine the increment of the *d*-spacing in the GO
13 sheets through intercalation of the cationic organic. X-ray diffractograms of the aerogels were
14 obtained by Cu-K α radiation ($\lambda = 0.15418$ nm) with scanning rate of 0.2 degrees/min at room
15 temperature. XRD is performed on dried thin film of aerogels. The aerogel samples were cut into
16 thin disks prior to X-ray measurements. Bragg's equation, $\lambda = 2d \sin(\theta)$ where *d* is the layer
17 spacing and θ is the angle of diffraction, was used to compute the *d*-spacing for GO nano-sheets.

18 Fourier-transform infrared (FT-IR) spectroscopy was used to investigate the oxidation of
19 graphene, polymerization of benzoxazine and the interactions between benzoxazine and GO. FT-
20 IR spectra were obtained using a Bomem Michelson MB-100 FT-IR spectrometer with a dry air
21 purging unit and a deuterated triglycine sulfate detector at a resolution of 4 cm^{-1} .

22 Textural morphology of the aerogels was observed with Scanning Electron Microscopy
23 (SEM) and Transmission Electron Microscopy (TEM). SEM analysis was performed with a FEI

1 Quanta 250 (FEG), coupled with Energy Dispersion X-Ray Spectroscopy (EDS). Regarding
2 sample preparation, a thin slice (~1.5 mm) cut on the vertical axis of each of the cylindrically
3 shaped specimens was mounted on standard aluminum SEM stabs using conductive silver glue.
4 TEM analysis was performed with a FEI Tecnai G20, coupled with EDS and a Gatan GIF 963
5 energy filtered camera. Samples were crushed using a mortar and pestle and then dispersed in
6 high purity ethanol (99.99 %) in an ultrasonic bath for ~30 s. A drop of the dispersed phase
7 would be deposited on Cu grid covered with a thin layer of amorphous carbon (lacey carbon),
8 following which the grid would be immediately transferred to the TEM holder to avoid
9 contamination.

The apparent bulk density (ρ_b) of the aerogel was obtained from the aerogel mass (m) and its volume (V) as described in Eqn. (1)

The values of skeletal density (ρ_s) were obtained by using helium in gas-displacement pycnometer. The apparent porosity percentage of the aerogels was calculated according to the following relation.⁴⁴

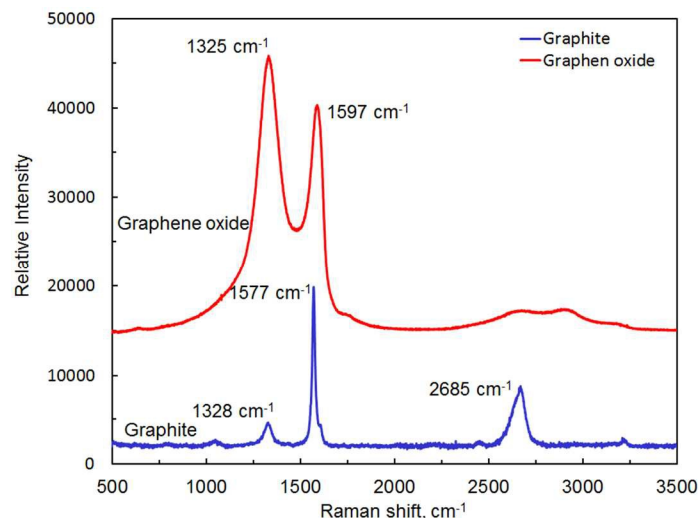
$$17 \quad \text{Porosity \%} = \left(1 - \frac{\rho_b}{\rho_s}\right) * 100 \quad \dots \dots \dots \quad (2)$$

The thermal stability of the aerogels were evaluated by thermogravimetric analysis (TGA) and differential thermogravimetric analysis (DTGA) using a TA Instruments High Resolution 2950. A sample (5-10 mg) from each obtained aerogel was placed in a platinum pan and heated from room temperature to 900 °C at a temperature ramp rate of 10 °C min⁻¹ under nitrogen atmosphere with a gas flow rate of 60 mL min⁻¹.

1 **3. RESULTS AND DISCUSSION**2 **3.1. Preparation of graphene oxide (GO)**

3 The oxidation of graphite has been confirmed by Raman spectroscopy and FT-IR. As shown in
4 Fig. 2, the Raman spectrum of natural graphite exhibits strong lines at 1577 cm^{-1} and 2685 cm^{-1} ,
5 which are assigned to the G band and 2D band, respectively, while the D band is shown as a
6 weak band at 1328 cm^{-1} .^{39,47,48} The two most intense lines appearing at 1597 cm^{-1} and 1330 cm^{-1} for
7 GO correspond to the G and D bands, respectively.³⁴ As shown in the GO spectra, the D band
8 shifts to higher frequency and becomes prominent. The ratio of D to G band intensity (I_D/I_G)
9 equals to 1.27, indicating the reduction in the average size of sp^2 domains due to extensive
10 oxidation.^{34,48}

11



12

13 **Fig. 2** Raman spectra of graphite (lower spectrum) and GO (upper spectrum).

14

15 FT-IR results confirm the introduction of oxygen-based functional groups on the basal plane
16 and edge of graphene (Supporting Information, Fig. S1). Expectedly, there is no significant peak
17 found in the natural graphite spectrum, while the spectrum of GO shows characteristic band at

1 3380 cm⁻¹ (the OH stretching mode), 1720 cm⁻¹ (the C=O stretching mode of carboxylic acid
2 groups), 1209 cm⁻¹ (=C-OH stretching vibrations) and 1043 cm⁻¹ (C-O stretching vibrations).
3 These results are in agreement with reported literature.³⁴⁻³⁷

4 **3.2. Interactions of GO and polybenzoxazine**

5 Recently, much attention has focused on the development of benzoxazines-based nanocomposite
6 materials.^{29,30} However, interaction of GO with benzoxazine containing functional groups have
7 not yet been reported. GO contains several reactive moieties on the surface of its nanosheets
8 including epoxide, hydroxyl, and carboxyl groups.^{34,36,41} The interactions between benzoxazine
9 and epoxy during the polymerization have been investigated.^{49,50} Jubsilp et al.⁵⁰ reported that
10 DSC thermograms of benzoxazine/epoxy blends showed at least two possible reactions: **(i)** the
11 exothermic peak due to polymerization of benzoxazine monomers. Phenolic structure is an
12 initiator and catalyst for polymerization of both benzoxazine⁴⁹⁻⁵¹ and epoxy⁵². **(ii)** The reaction
13 between the epoxide groups on the epoxy with the phenolic hydroxyl groups on
14 polybenzoxazine. Accordingly, we suggest that epoxy groups on the surface of GO sheets attach
15 the polybenzoxazine structure during the polymerization step. Furthermore, hydrogen bonding
16 between the polar groups on both polybenzoxazine and GO may take place. The proposed
17 interactions between SLTB(4HBA-t403) as aldehyde-terminal benzoxazine and GO are shown in
18 Schemes 3 and 4, while FT-IR was used to confirm these interactions.

19 The structure of SLTB(4HBA-t403) benzoxazine monomer was confirmed with ¹H-NMR
20 and FT-IR as shown in the Supporting Information Fig. S2 and S3, respectively; detailed
21 discussion can be found in S2.2. FT-IR was used to study the polymerization behaviour of
22 SLTB(4HBA-t403)/GO nanocomposite aerogels. A typical FT-IR profiles of neat SLTB(4HBA-
23 t403) at 75 °C and SLTB(4HBA-t403)/GO-5% aerogel at various temperatures (60, 160, 200 and

1 900 °C) are shown in the Supporting Information, Fig. S4. FT-IR spectrum of pristine GO
2 (Supporting Information, Fig. S1) indicates that the hydroxyl functional groups on the surface of
3 graphene sheets have characteristic band at 3380 cm⁻¹ (the OH stretching mode). FT-IR results of
4 SLTB(4HBA-t403) (Supporting Information, Fig. S4a) reveals that there is no absorption in the
5 range 3400-3000 cm⁻¹. After dispersion of GO in SLTB(4HBA-t403) matrix, a broad band
6 appearing at 3465 cm⁻¹ indicates the presence of hydroxyl funtional groups (-OH) of GO.³⁴ The
7 frequency shift from 3380 cm⁻¹ to 3465 cm⁻¹ is likely due to the weakening of OH hydrogen
8 bonds caused by the more hydrophobic environment of GO surrounded by SLTB(4HBA-t403),
9 which is consistent with the exfoliated GO. The samples heated at higher temperatures show
10 more absorption intensities of this peak due to the newly created phenolic -OH groups in the
11 polybenzoxazine chains. The phenolic hydroxyl group is also confirmed by the appearance of
12 new absorption peak around 3300 cm⁻¹.⁷

13 From the Supporting Information Fig. S4, it is obvious that the characteristic bands of the
14 GO functional groups heavily overlap with this newly generated OH band and it makes difficult
15 to study the interaction of GO and benzoxazine by FT-IR. The problem is compounded by the
16 low concentration of GO compared to the amount of polybenzoxazine matrix in all samples
17 studied. Therefore, further experiments were performed to confirm SLTB(4HBA-t403)/GO
18 interactions. The investigation of interfacial interactions between SLTB(4HBA-t403) and GO
19 were evaluated by FT-IR using sample with high concentration of GO (SLTB(4HBA-t403)/GO
20 is 40/60 weight percent), which forms a thin-layer of SLTB(4HBA-t403) on GO nanosheets.

21 The sample was prepared by blend of a concentration of benzoxazine (40 wt %) and GO (60
22 wt %) and thoroughly mixed for one min. The solution was casted on KBr pellet and dried at

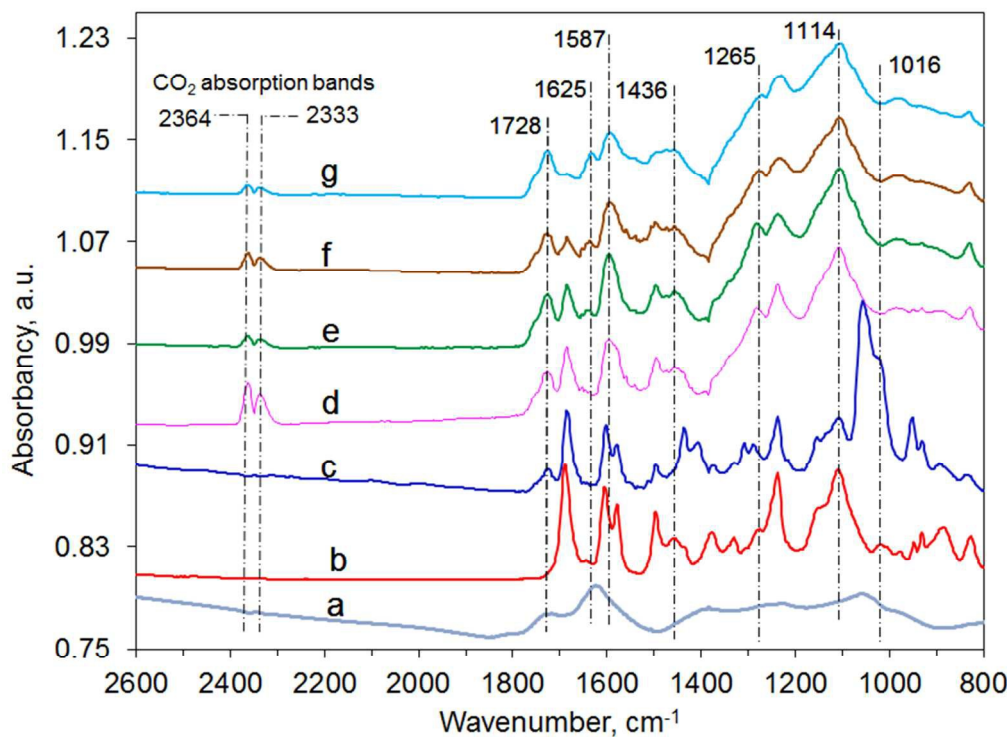
1 room temperature for FTIR measurements. Then, the casted film was subjected to a ring-opening
2 polymerization of benzoxazine monomer schedule of 2 h at each 100, 125, 175 °C.

3 Fig. 3 shows FT-IR spectra of neat GO, neat SLTB(4HBA-t403), and treated SLTB(4HBA-
4 t403)/GO nanocomposite at various temperatures. The FT-IR characteristics of GO are
5 separately discussed in detail (Supporting Information, Fig. S1). The important characteristic
6 infrared absorptions of the neat SLTB(4HBA-t403) structure are clearly observed as discussed
7 (Supporting Information, S2.2 and Fig. S3). The FT-IR spectrum of adsorbed layer of
8 SLTB(4HBA-t403) on GO sheets (Fig. 3c) shows a characteristic absorption band at 1728 cm⁻¹,
9 which is attributed to the C=O stretching band of carboxylic acid-functional groups of GO.^{34,53}
10 This peak slightly changed with heat treatment due to functional groups attached to the carbonyl
11 with a benzene ring or double bond in conjugation with carbonyl.⁵⁴ The results in Fig. 3c reveal
12 that mixing of GO to SLTB(4HBA-t403) significantly shifts the absorption band at 1114 cm⁻¹ of
13 polyether chain to lower wavenumber due to hydrogen bonding with the adsorbed water on the
14 GO-functional groups. After thermal treatment from 100 °C up to 175 °C, this band returned to
15 the same position (Fig. 3b) due to the evaporation of moisture.

16 Moreover, the ester-linkage formation in benzoxazine/epoxy resin blend system has been
17 reported.⁴⁹ The characteristic FT-IR bands of epoxy band (around 950-900 cm⁻¹) overlap with the
18 absorption bands of benzoxazine, making it difficult to follow the disappearance of epoxy bands
19 upon polymerization. However, the observation of the relative increase in the band at 1728 cm⁻¹
20 is due to ester group formation. More recently, chemical interaction of GO with phenolic resin
21 has been reported.⁵⁵ Zhou et al.⁵⁵ documented that esterification reaction occurred between
22 hydroxyl groups (-OH) on resole and carboxyl groups (-COOH) on GO, as confirmed by the
23 absorption band at 1722 cm⁻¹. Therefore, herein, the absorption band at 1728 cm⁻¹ is attributed to

1 the esterification reaction between phenolic –OH and carboxylic groups of GO after heat
2 treatment. In addition, the absorption bands at 2333 and 2364 cm⁻¹ are assigned to CO₂ as a
3 result of the oxidation of aldehyde groups.⁵⁶ In aldehyde-functional benzoxazines, oxidation of
4 aldehyde groups to form carboxylic groups has been reported.⁵⁶ Therefore, ester formation
5 resulting from carboxylic groups-epoxy reaction possibly occurred as seen in Scheme 3a. In this
6 case of oxidation of aldehyde groups, the released CO₂ would present a great advantage to
7 partially contribute to the porous structure of the aerogels, further investigation will be discussed
8 in details elsewhere.⁵⁷

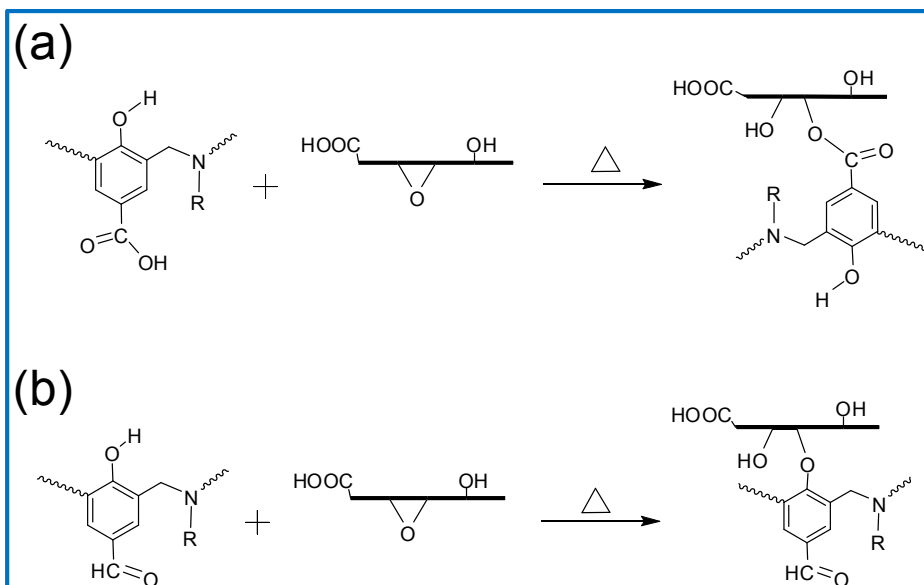
9



10
11 **Fig. 3** FT-IR spectra of interfacial interaction of GO and SLTB(4HBA-t403): (a) neat GO, (b)
12 neat SLTB(4HBA-t403), (c), (d), (e), and (f) SLTB(4HBA-t403)/GO (40/60 weight percent) at
13 25, 100, 125, and 175 °C, respectively.

14

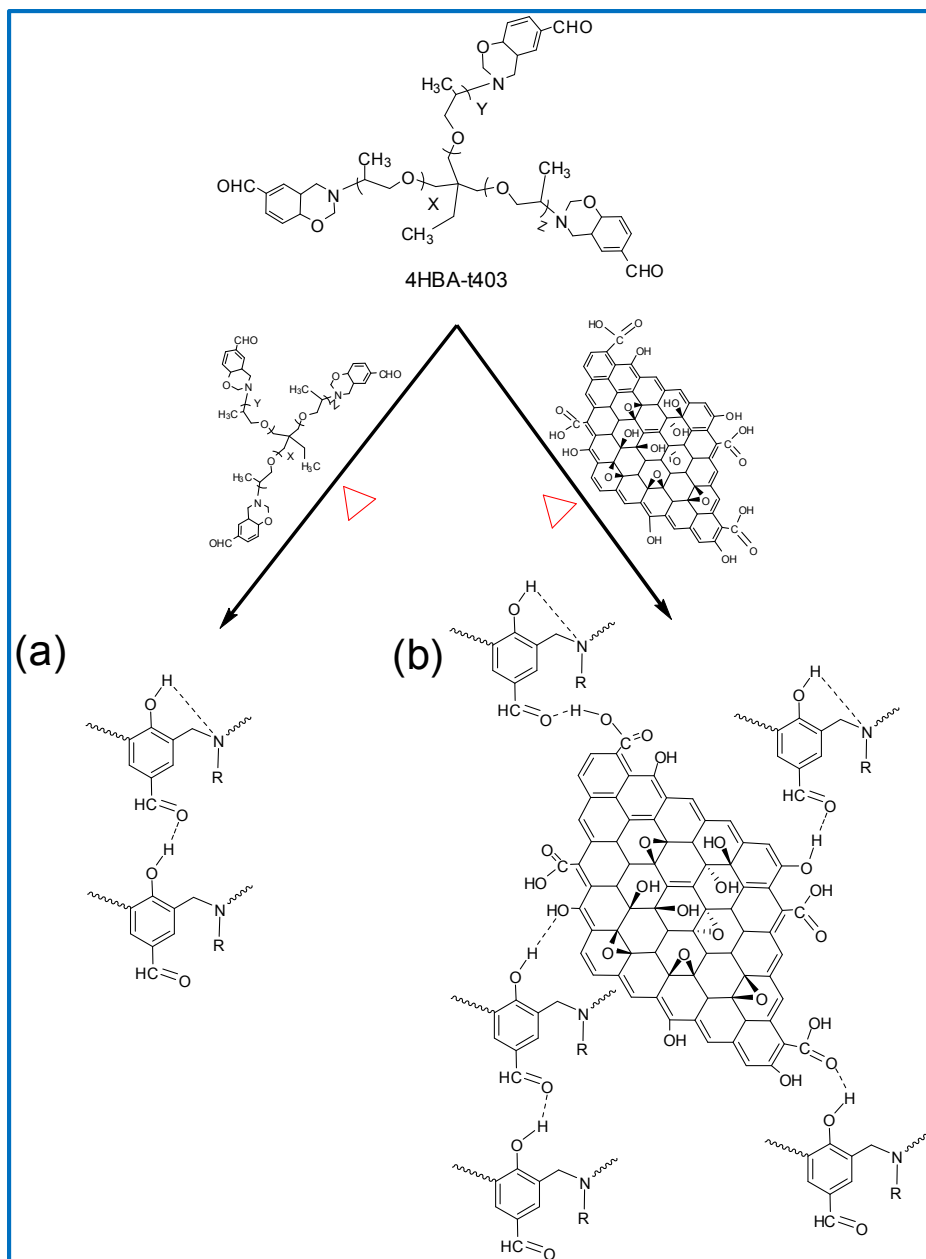
15



1 **Scheme 3** Proposed chemical interaction between SLTB(4HBA-t403) and GO: **(a)**
2 Esterification-based on carboxylic acid of oxidized aldehyde-functional benzoxazine and **(b)**
3 Etherification-based on the residual aldehyde-functional benzoxazine.
4
5

6 Furthermore, during heat treatment of ring-opening polymerization of benzoxazine, the
7 produced phenolic hydroxyl is proposed to react with epoxy groups of GO (etherification). The
8 polyether band at 1114 cm^{-1} became a broader peak and overlapped with 1161 cm^{-1} , which
9 attributed to the chemical attachment of polybenzoxazine with GO via phenolic hydroxyl-epoxy
10 reaction as proposed in Scheme 3b. The resulting absorption band increased with increasing heat
11 treatment due to production of phenolic hydroxyl $-\text{OH}$. The absorption bands in the range $1608-$
12 1583 cm^{-1} in the FT-IR spectra of SLTB(4HBA-t403)/GO nanocomposites become overlapped
13 bands due to newly appeared $\text{C}=\text{C}$ band from thermal treatment of GO.³⁰ Heat treatment of GO
14 partially decomposes the functional groups resulting in aromatic conjugated bonds of graphene.

Published on 20 October 2015. Downloaded by University of Cambridge on 26/10/2015 05:50:50.



1
2 **Scheme 4** Proposed hydrogen bonding network formed between oxygen-functionality on GO
3 and SLTB(4HBA-t403): (a) Hydrogen bonding in polymerized aldehyde-functional benzoxazine
4 [Adapted from ref. 56] and (b) Hydrogen bonding in polymerized SLTB(4HBA-t403)/GO.

5
6 Hydrogen bonding is possible between the aldehyde-functional benzoxazines and GO
7 formed. Polybenzoxazines contain extensive—intermolecular and intramolecular hydrogen

1 bonding between phenolic hydroxyl –OH and electronegative atoms such as O and N.^{7,56,58-60}

2 Also, hydrogen bonding interaction between the aldehyde groups and polybenzoxazine has been

3 reported as seen in Scheme 4a.⁵⁶ In the polymerized aldehyde-functional benzoxazine monomer,

4 the aldehyde groups contain electronegative O atoms, which can form intermolecular hydrogen

5 bonding with H atoms of phenolic hydroxyl groups. Herein, the H atoms of hydroxyl groups of

6 GO may show similar tendency (Scheme 4b). Fig. S5 shows the infrared spectra of the C=O

7 stretching (aldehyde groups) of SLTB(4HBA-t403) and SLTB(4HBA-t403)/GO samples. The

8 neat SLTB(4HBA-t403) gives a carbonyl absorption peak at 1688 cm⁻¹ (Fig. S5b).^{56,58,59} After

9 adding the GO into the SLTB(4HBA-t403) system (Fig. S5c), the carbonyl stretching frequency

10 is shifted into 1683 cm⁻¹, corresponding to the hydrogen bonded aldehyde groups of

11 SLTB(4HBA-t403) with functional groups on GO sheets as described in Scheme 4b. This new

12 band (1683 cm⁻¹) gradually shifts into the hydrogen bonded carbonyl (1633 cm⁻¹) with increasing

13 heat treatment of nanocomposite sample (SLTB(4HBA-t403)/GO).⁵⁸ These results suggest that

14 there interaction in the residual aldehyde groups of polybenzoxazine resins. These results are in

15 agreement with literature.⁵⁶ As seen in Fig. S5, the existence of hydrogen bonding makes the

16 frequency of the C=O band (1683 cm⁻¹) decrease in the FT-IR spectrum. The hydrogen bonding

17 results from the interaction of electronegative atoms in the residual aldehyde groups with H

18 atoms of hydroxyl groups of both GO and polybenzoxazine. Also, the phenolic hydroxyl groups

19 of benzoxazine may form hydrogen bonding with hydroxyl groups of GO. Further hydrogen

20 bonding may occur between carboxylic groups of GO and H atoms of polybenzoxazine (–OH

21 and –COH). According to these results, one can conclude that polymerized SLTB(4HBA-

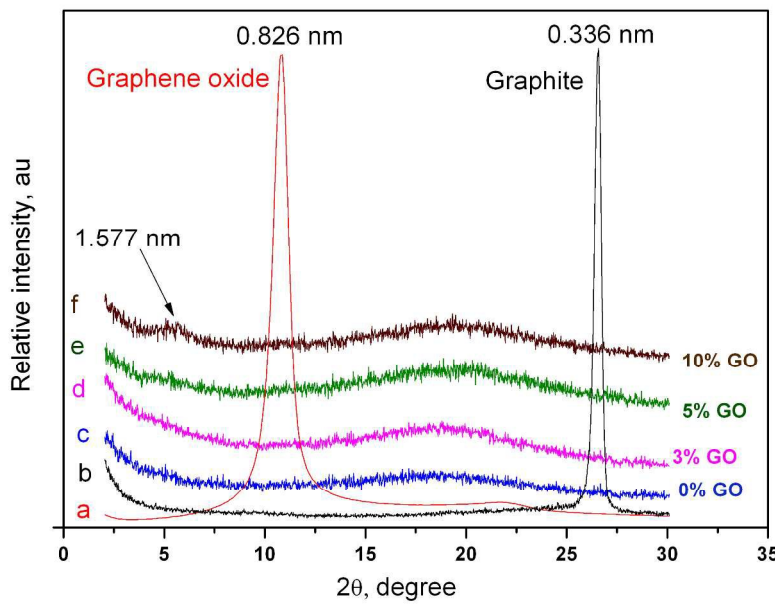
22 t403)/GO contains a large amount of intermolecular hydrogen bonding formed by residual

23 aldehyde and phenolic hydroxyl groups with oxygen-functional groups of GO (Scheme 4).

1 Alhikari⁶¹ et al. reported that functional groups (-OH, -COOH) are able to form hydrogen bonds
2 with other molecules under appropriate conditions. As result of hydrogen bonds, polymers can
3 be assembled with GO to form a hydrogel matrix.^{43,62} To conclude the FT-IR results,
4 incorporation of neighboring group of aldehyde moieties in benzoxazine monomers play a role
5 for providing more interaction sites during hybridization of polybenzoxazine with GO. These
6 interactions contribute to the enhanced performance of the aerogels as a new class of
7 nanocomposite aerogels. The strong interaction of benzoxazine chains with GO nanosheets leads
8 to high performance nanocomposites-based materials.

9 3.3. X-ray diffraction analysis (XRD)

10 Fig. 4 displays the X-ray diffractograms of graphite, GO, and the nanocomposite aerogels. In the
11 case of oxidation of the neat graphite, the d_{002} diffraction peak in the natural graphite shifted
12 from around $2\theta = 26^\circ$ to lower 2θ values, indicating the GO formation.^{34,36,38,63}



13
14 **Fig. 4** XRD diffractograms of profiles of: (a) GO, (b) graphite, (c) , (d) , (e), and (f) of
15 SLTB(4HBA-t403)/GO nanocomposites with various GO contents of 0 wt%, 3 wt%, 5 wt%, and
16 10 wt% GO, respectively.

1 The results show that the *d*-spacing of graphene layers was increased from 0.34 nm to 0.83
2 nm after the oxidation process due to the formation of oxygen-functional moieties which are
3 acting as spacers. The challenges are to achieve molecule-level dispersion and maximum
4 interfacial interaction between the nanofiller and the polymer matrix at low loading. The XRD
5 pattern of neat SLTB(4HBA-t403) (Fig. 4c) shows a typical diffraction of an amorphous polymer
6 with a broad peak at $2\theta = 18^\circ$. In the case of SLTB(4HBA-t403)/GO aerogels, the effect of
7 SLTB(4HBA-t403) on exfoliation of GO also has been evaluated. Up to 5 wt% of GO, no
8 obvious diffraction peak is seen below $2\theta = 10^\circ$. This means that GO may be fully exfoliated in
9 polybenzoxazine matrix due to the strong interaction between GO and SLTB(4HBA-t403),
10 although the concentration of GO is so low and verification of complete exfoliation only by
11 XRD is difficult. However, the aerogel containing 10 wt% GO shows a broad diffraction peak at
12 $2\theta = 5.6^\circ$, indicating that polybenzoxazine has intercalated fraction of GO. Observation of
13 intercalated fraction implies the trend to aggregate the nanoparticles starts around this
14 concentration. As a result of polybenzoxazine intercalation, the *d*-spacing of GO increased from
15 0.826 nm to 1.58 nm.

16 **3.4. Morphological and microstructure analysis of GO reinforced aerogels**

17 Effects of hybridization of SLTB(4HBA-t403) matrix with GO on morphology and structure of
18 benzoxazine aerogel have been investigated. The density and porosity of all obtained aerogels
19 are summarized in Table 1. Slightly differences were observed in physical structures of neat and
20 nanocomposite polybenzoxazine aerogels. The apparent density (ρ_b) and porosity of the obtained
21 aerogels are in the range of 0.1482–0.1550 g cm⁻³ and 84.50–86.52 %, respectively. These results
22 confirmed highly porous structure of the hybrid aerogels.⁴⁴ The results indicated that bulk
23 density (ρ_b) of neat polybenzoxazine aerogel is higher than the nanocomposite aerogels, which

1 can be related to their microstructures behavior as shown in Fig. 5. By comparing SEM
2 micrographs for the neat polybenzoxazine and nanocomposite aerogel (SLTB(4HBA-t403)/GO-
3 5%), samples containing GO have more overlapping layers in the morphology than GO-free
4 aerogels. This increase in the number of layers may lead to the observed increase in the porosity
5 with increasing GO content.

6

7 Table 1 Bulk density and porosity of the obtained aerogels.

Sample code	Bulk density (g cm^{-3})	Porosity (%)
SLTB(4HBA-t403)/GO-0	0.1550	84.50
SLTB(4HBA-t403)/GO-1	0.1475	85.38
SLTB(4HBA-t403)/GO-3	0.1477	85.65
SLTB(4HBA-t403)/GO-5	0.1478	85.91
SLTB(4HBA-t403)/GO-10	0.1482	86.52

8

9
10 **3.4.1. Scanning Electron Microscopy (SEM)**

11 The morphology of polybenzoxazine aerogels has been reported earlier.^{13,15} To the best of our
12 knowledge, this is the first time reported in literature where morphology and microstructure of
13 polybenzoxazine/GO aerogels is studied with SEM. SEM analysis shows that all samples contain
14 a highly porous structure, a result of solvent removal; however, pore sizes do not exhibit uniform
15 distribution. The cross section of the polybenzoxazine aerogel is shown in Fig. 5a and 5b. The
16 cross section of the specimen containing 5% GO (SLTB(4HBA-t403)/GO-5%) is shown in Fig.
17 5c and 5d, while lateral sections are shown in Fig. 5e, 5f and 5g.

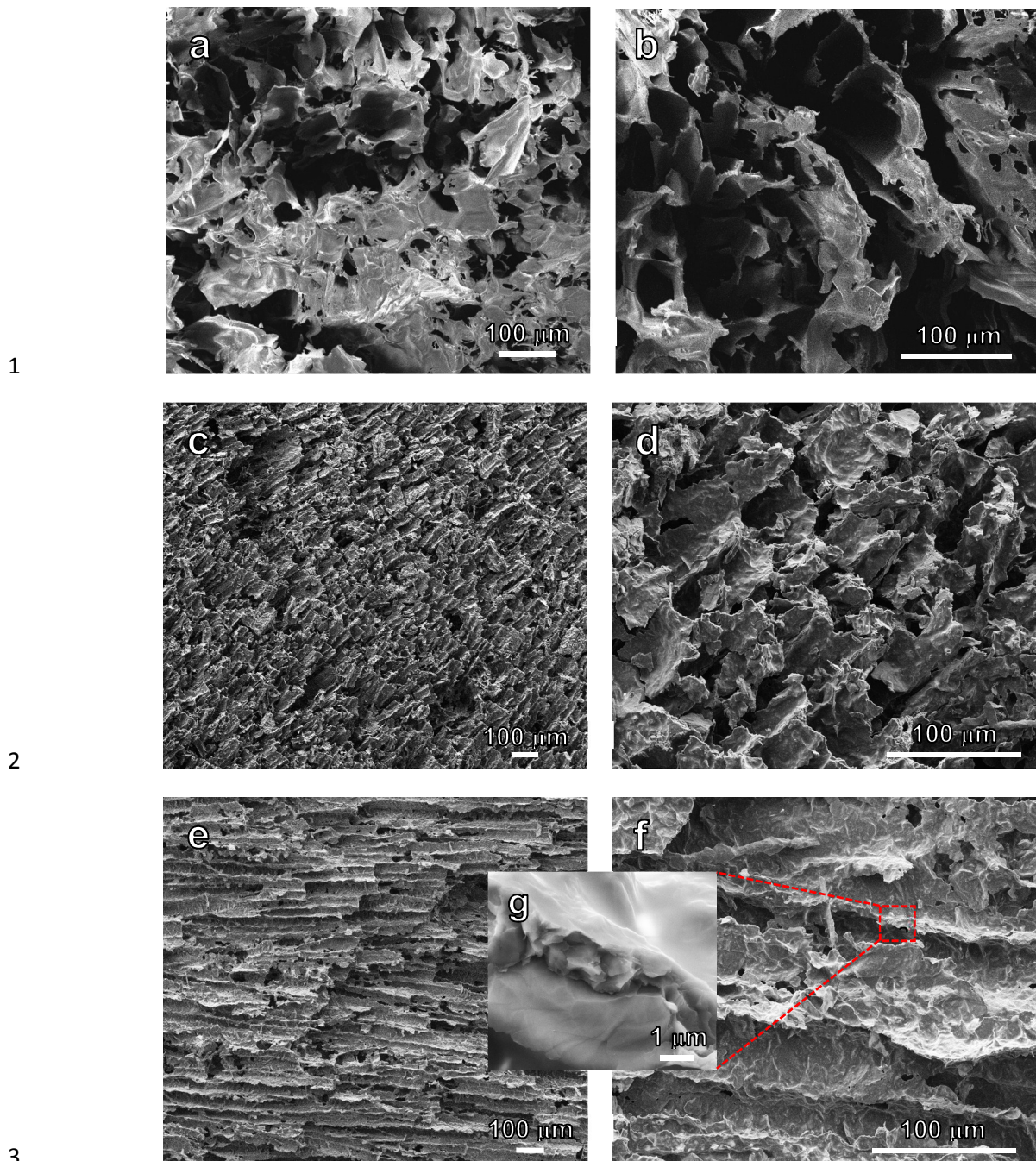
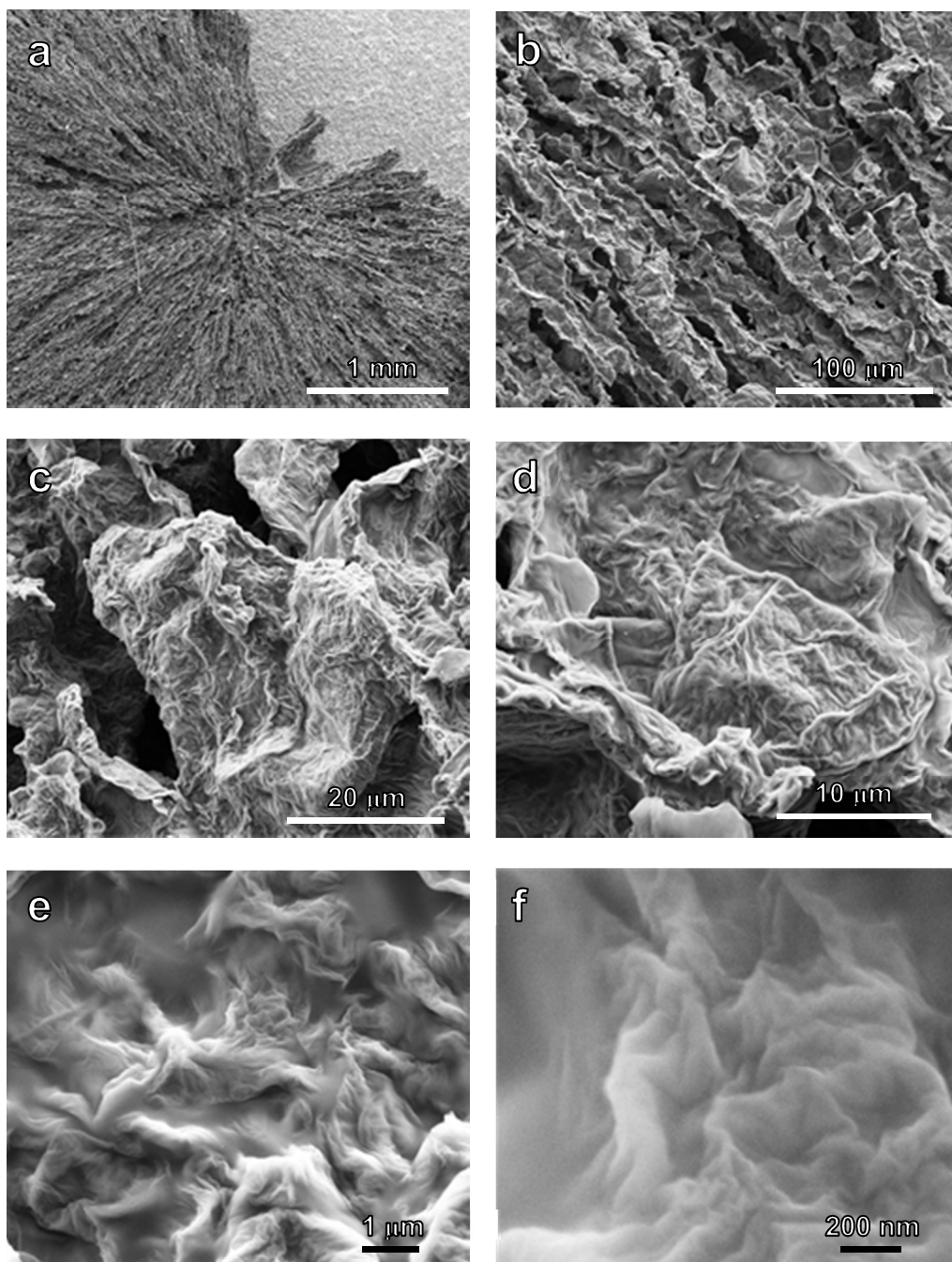


Fig. 5 SEM micrographs of polybenzoxazine-based aerogels at various microscope magnifications: (i) Cross-section images of polymeric aerogel without GO: (a) and (b). (ii) SLTB(4HBA-t403)/GO-5% aerogel: (c) and (d) cross-section, (e) and (f) lateral-section;(g) inset shows the fractured structure of the layer separating two aerogel pores.

1 It is clear that the pore structure of nanocomposite aerogels is different than that of the
2 organic aerogel as the pore sizes in polymeric aerogel (Fig. 5b) appear larger than those of the
3 GO reinforced aerogel (image 5d). The structure of pores is dependent on the size of the ice
4 crystals during the fabrication of the aerogels. During the freezing, as the ice crystals grow,
5 micro-ribbons form on the walls of the aerogel.^{1,45} The small size of ice crystal growth leads to
6 narrow pore, resulting in an increase in the surface area. In addition, the GO reinforced aerogels
7 exhibit a more layered structure than the polymeric aerogel as shown by SEM images of lateral
8 sections (side view) of the 5% GO reinforced aerogels (Fig. 5e, 5f, 5g). Furthermore, it is clearly
9 seen that the surface of the layers exhibits increased roughness.¹ In addition, the layers extend
10 through the length of the aerogel and connected together via strands to create irregular pores.
11 Fig. 5g illustrates the morphology of the fractured structure of edge between two aerogel pores at
12 high magnification ($\times 40000$ and scale of 3 μm). The inner surface of the fracture is very different
13 from that of the outer surface due to the presence of the nanofiller. It is interesting to note that
14 the center area shows rough appearance with what appears as a hierarchical structure, while the
15 GO is distributed on the interior surface of the layer without any aggregation.

16 Carbon aerogels possess large surface area, which have advantages in catalysis and
17 adsorption applications⁶⁴ as well as electrodes for supercapacitors.¹⁶ Morphological behavior of
18 carbon aerogels has been extensively studied using SEM.^{16,42,43} Polybenzoxazine-based carbon
19 aerogels and xerogels have been investigated.^{16,17} Herein, morphology of carbon neat
20 polybenzoxazine and polybenzoxazine/GO nanocomposites aerogels studied. Fig. 6 contains the
21 SEM micrographs of carbonized SLTB(4HBA-t403)/GO-5% aerogel. Fig 6b reveals that the
22 surface layers become coarser after carbonization. The high magnification SEM images (Fig. 6c,
23 d, and e) show surface topology becomes irregularly wrinkled upon carbonization.

1



2

3

4

5

Fig. 6 SEM micrographs of poly(SLTB(4HBA-t403)/GO-5%) carbon aerogels at different microscope magnifications.

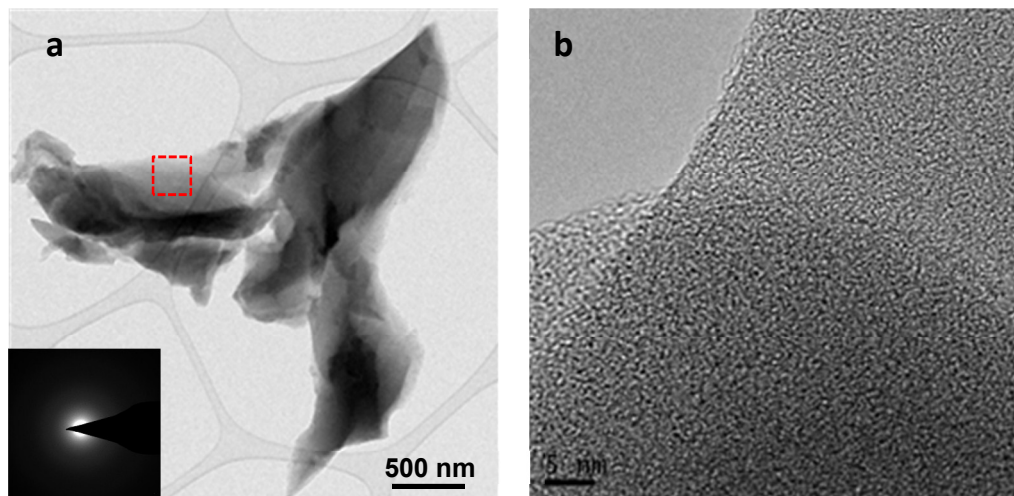
1 The possible contribution to these wrinkles may be the crumpling of graphene nanosheets
2 that result from the reduced GO and after the decomposition of soft segments of
3 polybenzoxazine. Therefore, random distribution of GO sheets can be observed (image 6f). The
4 observations made with SEM are in good agreement with XRD results which show that GO is
5 highly exfoliated in the polymeric matrix.

6

7 **3.4.2. Transmission Electron Microscopy (TEM)**

8 The structure and morphology of as-prepared polybenzoxazine/GO aerogels were also
9 investigated by means of transmission electron microscopy (TEM). TEM images of the neat
10 poly(SLTB(4HBA-t403)) are shown in Fig. 7, while TEM images of polymerized and
11 carbonized SLTB(4HBA-t403)/GO-5% aerogels are shown in Fig. 8 and 9 respectively.

12



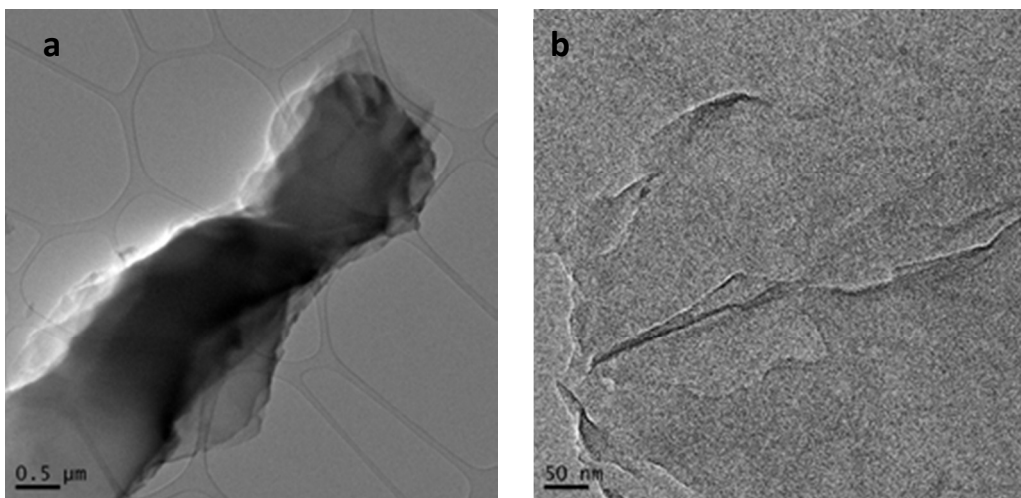
13 **Fig. 7** TEM (a) and HRTEM (b) images of poly(SLTB(4HBA-t403)) aerogel; inset: SAED
14 pattern (collected at area marked with red rectangle) reveals no crystalline structure.

15

16 TEM analysis revealed the wide distribution of size and shape observed for the pores of
17 the polybenzoxazine aerogel. Furthermore, the amorphous nature of the specimen was confirmed

1 with Selected Area Electron Diffraction (SAED) and High Resolution TEM (HRTEM). Similar
2 finds have been previously reported for neat polybenzoxazine-based porous carbons.^{16,17} EDS
3 analysis showed minor presence of Cl impurities (>0.1%).

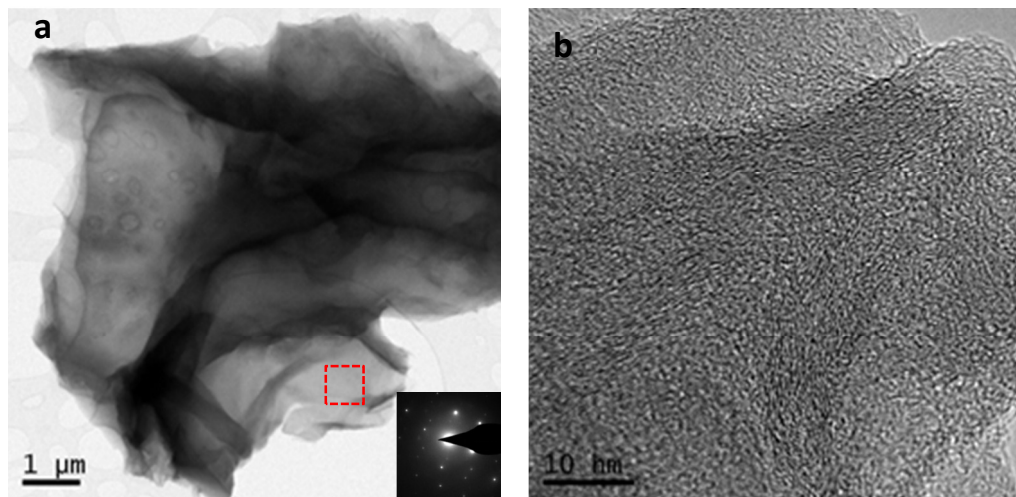
4



5 **Fig. 8** TEM images of SLTB(4HBA-t403)/GO-5% polymerized aerogel; (a) low magnification,
6 (b) high magnification.

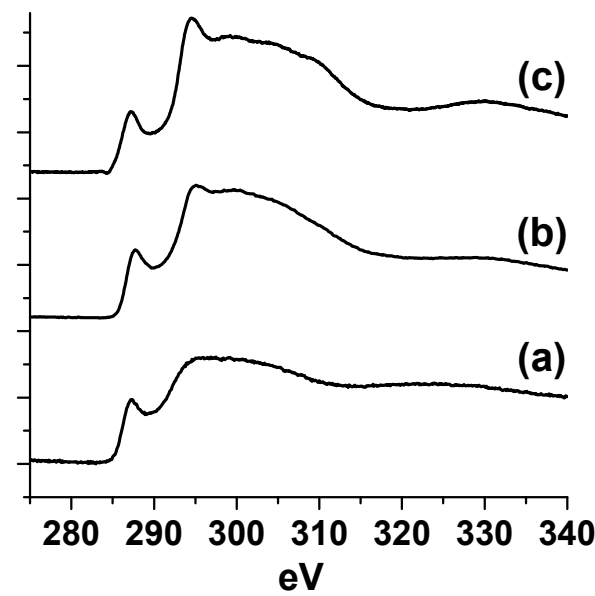
7

8 Fig. 8 shows TEM micrographs of SLTB(4HBA-t403)/GO-5% polymerized aerogel.
9 Concerning the polymerized SLTB(4HBA-t403)/GO-5% aerogel, its morphology is similar to
10 the polybenzoxazine aerogel, exhibiting a wide distribution of pore size and shape. Thin carbon
11 layered structures with no aggregation of GO were observed, as expected from previous work by
12 Alhassan et al.³⁰ Overall, the GO sheets were found to be homogeneously dispersed into the
13 polybenzoxazine amorphous structure. Similar finds are observed for the carbon aerogel
14 containing 5 wt % GO, although in this case the ordering of the GO sheets appeared to be higher;
15 this was observed with HRTEM analysis at the edge of particles, where turbostratic and graphitic
16 layers were observed (see Fig. 9b).⁶⁵



1 **Fig. 9** TEM images of SLTB(4HBA-t403)/GO-5% carbon aerogel: (a) low magnification, (b)
2 high magnification; inset: SAED pattern (collected at area marked with red rectangle) reveals an
3 exist crystalline structure due to presence of GO.

4



5

6 **Fig. 10** Background subtracted and deconvoluted EELS spectra at carbon K-edge for
7 poly(SLTB(4HBA-t403)) aerogel (a), SLTB(4HBA-t403)/GO-5% polymerized aerogel (b) and
8 SLTB(4HBA-t403)/GO-5% carbon aerogel (c).

1 A strong indication of the increased GO presence was provided with EELS analysis,
2 shown in Fig. 10. Specifically, carbon hybridization was evaluated by acquiring the C K-edge for
3 the three specimens mentioned above: poly(SLTB(4HBA-t403)) aerogel, SLTB(4HBA-
4 t403)/GO-5% polymerized aerogel and SLTB(4HBA-t403)/GO-5% carbon aerogel. The
5 characteristic peaks corresponding to sp^2 hybridization ($1s \rightarrow \pi^*$ at 284eV and $1s \rightarrow \sigma^*$ at
6 291eV) are more prevalent in the carbonized and polymerized aerogels, due to GO presence in
7 the matrix. On the other hand, the polybenzoxazine aerogel exhibits significantly lower sp^2
8 hybridization, which is mostly attributed to its amorphous nature.

9 The overall of microstructure analysis can be summarized as the GO sheets were found to
10 be homogeneously distributed into the polybenzoxazine aerogels. In addition, GO enhances the
11 microstructure and reduces the pore size of polybenzoxazine aerogels, while the surface topology
12 of GO/polybenzoxazine aerogel becomes irregularly wrinkled upon carbonization due to the
13 unique structure of GO.

14

15 **3.5. Effect of GO on polymerization behavior of benzoxazine monomer**

16 The influence of GO content on the polymerization behavior of benzoxazine monomer was
17 monitored and analyzed by DSC. As seen in Fig. 11, the heat treatment of neat SLTB(4HBA-
18 t403) and pristine GO showed only one exothermic peak at 207 and 205 °C, respectively. The
19 similarity of these two maxima is purely accidental. On the other hand, SLTB(4HBA-t403)/GO
20 aerogels showed multiple overlapped or separated exothermic peaks with lower onset
21 temperatures. This observation suggests that polymerization pathway of SLTB(4HBA-t403)/GO
22 nanocomposites is different comparing with the neat SLTB(4HBA-t403). This is hypothesized to
23 be due to the catalytic effect caused by the surface species of GO.

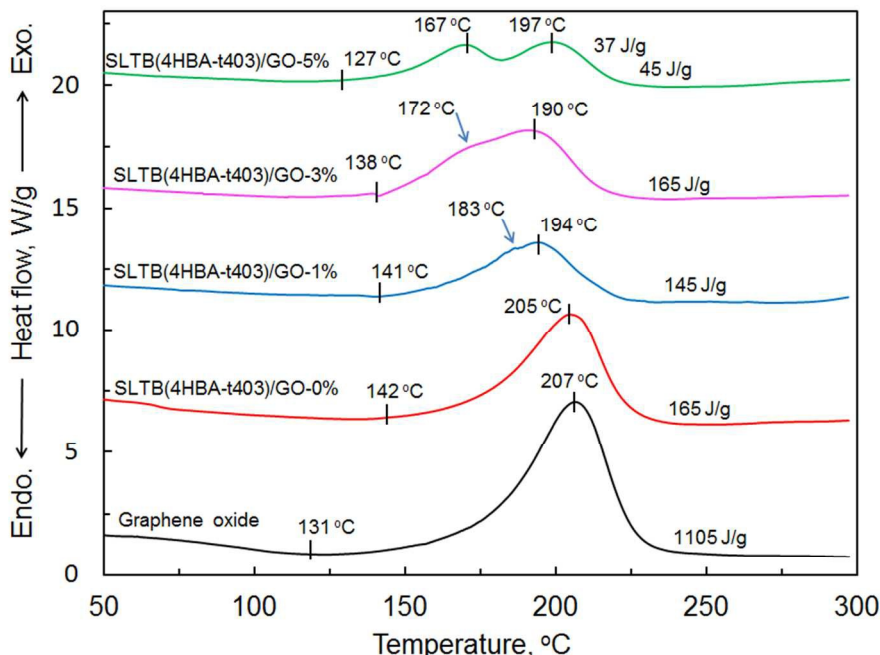


Fig. 11 DSC thermograms of SLTB(4HBA-t403)/GO aerogels with different GO content.

It has been reported that both phenolic and carboxylic groups exist on the GO surface.⁶⁶ Also, both phenolic and carboxylic acids are effective benzoxazine polymerization initiators and/or catalysts.^{51,67} As a result, increase in the GO contents decreases the onset polymerization temperature of the SLTB(4HBA-t403)/GO aerogels. The recent report by Gu et al.²⁹ demonstrated that GO has a catalytic effect on the ring-opening polymerization of benzoxazine; however, their DSC investigation did not show de-oxygenation peak of GO. On the other hand, the exothermic peak of GO at 207 °C observed in this study is in agreement with reported results.^{60,68} Zhao et al.⁶³ found that de-oxygenation of GO has a large single exothermic peak at 200 °C. Furthermore, Alhassan et al.³⁰ reported two exothermic peaks for benzoxazine/GO nanocomposites. It is noteworthy to mention that presence of GO in all cases has catalytic effect on the ring-opening polymerization of the benzoxazine monomer. The results in Fig. 11 reveal that the maximum temperature of the polymerization exotherm on DSC and the area under the

1 peak are significantly shifted to lower values. As an example, 5 wt% GO the onset temperature
2 and maximum temperature of neat SLTB(4HBA-t403) decreased from 142 and 207 °C to 127
3 and 167 °C, respectively, indicating that GO has significant catalytic activity on benzoxazine
4 polymerization.

5 DSC results also show that addition of GO to benzoxazine matrix has catalytic effect on
6 reducing the polymerization enthalpies of aldehyde-terminal benzoxazine monomer. Neat
7 aldehyde-terminal benzoxazine and GO show exotherm with enthalpies of 165 and 1105 J/g,
8 respectively. Accordingly, for instant, theoretical values of enthalpies for benzoxazine
9 polymerization of samples containing 1% and 3% of GO should read 174 and 193 J/g,
10 respectively. However, the DSC results indicated that the polymerization enthalpies of same
11 nanocomposite samples are 145 and 165 J/g, respectively.

12

13 **3.6. Thermal stability of GO reinforced aerogels**

14 Polybenzoxazine-based porous materials including aerogels exhibit anomalous thermal
15 stability.^{6,15,17} Lorjai et al.⁶ studied the thermal decomposition of neat polybenzoxazine in
16 comparison to the corresponding aerogel. Polybenzoxazine aerogel exhibited a much higher
17 degradation temperature and char yield than the corresponding bulk polybenzoxazine. Thermal
18 stability of the obtained aerogels after polymerization was evaluated by TGA and DTG. TGA
19 profiles of pristine GO, poly(SLTB(4HBA-t403)) aerogel, and poly(SLTB(4HBA-t403)/GO)
20 aerogels are shown in Fig. 12 and the results are summarized in Table 2.

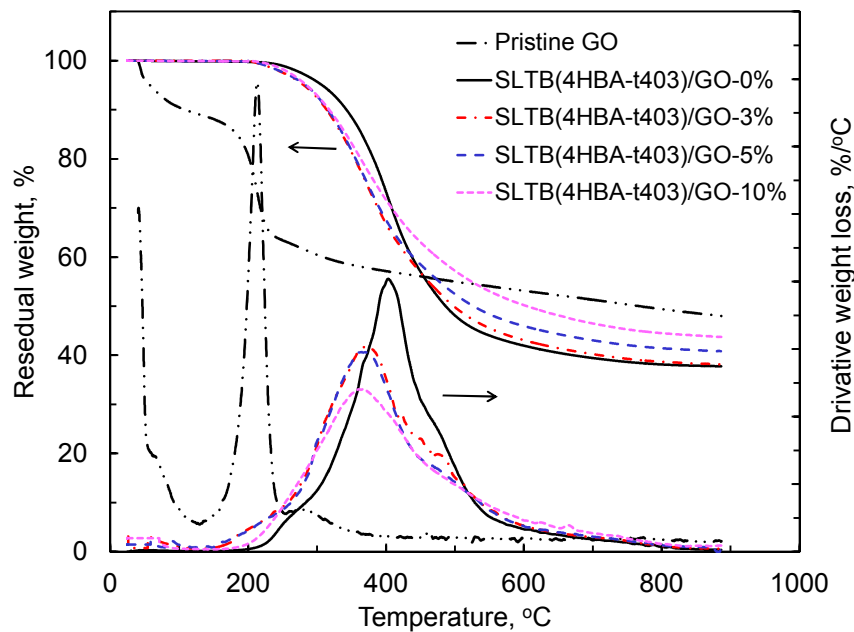


Fig. 12 TGA thermograms of aerogels obtained with different GO content.

Table 2 Summary of TGA data of the aerogels with different GO content.

Sample code	Temperature of Decomposition					
	T _{max} (°C)	T _{d5} (°C)	T _{d10} (°C)	T ₂₀ (°C)	T ₅₀ (°C)	Char Yield (%)
Neat GO	211	57	109	201	797	49 ± 1
0 wt% GO	396	304	341	382	396	37 ± 2
3 wt% GO	364	280	314	355	498	39 ± 2
5 wt% GO	365	283	316	356	527	42 ± 3
10 wt% GO	367	285	318	363	605	45 ± 2

The results indicate that the poly(SLTB(4HBA-t403)/GO) has weight loss at lower temperature than the neat poly(SLTB(4HBA-t403)) due to the low temperature weight loss of GO; however, the char yield is higher with GO because of the higher char yield of GO than

1 polybenzoxazine. TGA results of GO show two regions of weight loss. The first weight loss
2 occurred below 100 °C, which is due to the evaporation of the adsorbed moisture. The second
3 weight loss is ascribed to the decomposition of functional groups.⁶³

4 The results in Table 2 indicated that the maximum degradation temperature of neat GO is
5 211 °C, which is much lower than that for the neat polybenzoxazine. The lower degradation
6 temperature is attributed to the low thermal stability of soft segment of the functional groups of
7 GO. This investigation is in agreement with literature. The previous studies reported that the
8 thermal decomposition of instable oxygen-containing functional groups occurring at a
9 temperature of 200 °C.³⁴ The TGA results showed that stability of GO is shifted to about 400 °C
10 after incorporation with benzoxazine, which ascribed to the strong interaction of benzoxazine
11 structure with the functional groups of GO as early discussed.

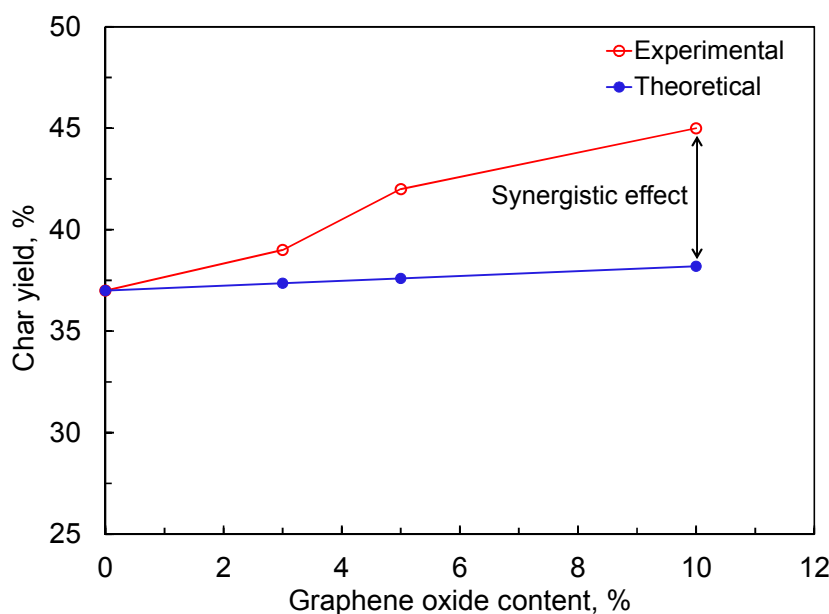
12 As seen in Table 2, the maximum rate degradation temperature (T_{\max}) of GO is 211 °C.
13 However, the 5, 10, 20 and 50 % weight loss temperatures (T_{d5} , T_{d10} , T_{d20} , and T_{d50}) of
14 poly(SLTB(4HBA-t403)/GO) aerogels increased with GO-loading. For example, T_{d5} and T_{d10} for
15 poly(SLTB(4HBA-t403)/GO-3%) are 280 and 314 °C, respectively, whereas T_{d5} and T_{d10} for
16 poly(SLTB(4HBA-t403)/GO-10%) are 285 and 318 °C. The improved properties of polymerized
17 nanocomposite aerogels may be due to the strong interactions with GO as discussed earlier.
18 Additionally, the GO reinforced aerogels exhibited much lower degradation behavior at higher
19 temperatures (>400 °C) than the neat polybenzoxazine aerogel, resulting in increased char yields,
20 which is important property for preparing carbon aerogels. As seen in Table 2, the char yield at
21 800 °C of polybenzoxazine aerogel increased from 37 to 45% by loading 10 wt% GO. The char
22 yield of GO is high since it is mostly carbon. Thus, increased the char yield of the obtained
23 samples is expected. Therefore, polybenzoxazine/GO aerogels not only exhibit improved

1 morphology than the neat polybenzoxazine aerogel, but also show excellent precursor for carbon
2 aerogels. The char yield of benzoxazine aerogels increased significantly with GO content,
3 primarily due to their strong interaction. To show the synergistic effect of GO-loading on the
4 char yield of polybenzoxazine aerogels, the theoretical char yield for each nanocomposite
5 aerogels was calculated. The theoretical char yield was obtained based on the composition of the
6 sample and the actual char yield for neat both GO and polybenzoxazine, poly(SLTB(4HBA-
7 t403)). The theoretical char yield value was calculated according to the Eq. (3):

$$M_{total}\% = X_{PBZ} M_{PBZ}\% + (1 - X_{PBZ})M_{GO}\% \quad \dots \quad (3)$$

10 Where:

11 M_{total} is the theoretical value of char yield. M_{PBZ} is the char yield during TGA run of neat
12 polybenzoxazine, PBZ. X_{PBZ} is the mass fraction of polybenzoxazine in the sample. M_{GO} is the
13 char yield during TGA run of neat GO.



14

15 **Fig. 13** Theoretical and measured char yield for polybenzoxazine aerogels with different GO
16 content.

1 In order to investigate whether interactions existed between aldehyde-functional benzoxazine
2 and GO, the theoretical and experimental values of char yield was compared. Fig. 13 displays the
3 expected and experimental char yields of the nanocomposite aerogels. The char yields of the
4 nanocomposites are higher than the theoretical prediction, which is attributed to the synergism
5 between polybenzoxazine and GO due to their strong interactions.

6 To summarize the TGA results, these nanocomposite aerogels derived from GO-reinforced
7 polybenzoxazine exhibit more efficient for carbon aerogels than aerogels obtained from neat
8 polybenzoxazine due to the increase in the char yield with increasing the GO content.
9 Furthermore, the PBZ aerogels are mechanically stable due to the unique feature of PBZ for
10 cross-linking ability.⁷ In addition, presence of aldehyde groups enhances PBZ/GO interactions as
11 investigated earlier. As a result of the network structure, the cross-linking contributes stiffness to
12 the aerogels. These advantages make PBZ/GO hybrid aerogels as one of the strong candidates of
13 aerogels for many applications.

14

15 **4. CONCLUSIONS**

16 Novel polybenzoxazine nanocomposites with three-dimensional (3D) porous materials have been
17 successfully prepared by blending of star-like telechelic aldehyde-terminal-benzoxazine
18 (SLTB(4HBA-t403)) with graphene oxide (GO) nanosheets. The 3D porous solids have been
19 developed via freeze-drying of various colloidal dispersion of SLTB(4HBA-t403)/GO.
20 Physicochemical interactions between aldehyde-terminal benzoxazine and GO interphases
21 matrices led to hybridization. These interactions between functional groups of both
22 SLTB(4HBA-t403) and GO are important in the formation of networks structure. FT-IR results
23 indicated that during the heat treatment of SLTB(4HBA-t403)/GO aerogels, the aldehyde groups

1 possibly oxidases and form carboxyl moieties. Therefore, ester formation results from chemical
2 interaction SLTB(4HBA-t403) and GO via -OH and -COOH moieties. Furthermore, a strong
3 hydrogen bonding is occurred between aldehyde-terminal benzoxazine and GO. The unique
4 combination of intramolecular and intermolecular hydrogen bonding contributes to the properties
5 of polybenzoxazine/GO aerogels. The XRD investigations indicated that GO is exfoliated in
6 benzoxazine matrix up to 5 wt%, while slight residual GO aggregation was observed with 10
7 wt% GO. Morphological studies show that the aerogels exhibit porous nanostructure features.
8 The presence of GO in polybenzoxazine aerogels plays a significant role in enhancing the
9 morphological properties. The SEM images reveal that GO increases the layered structure of the
10 aerogels and surface roughness. SEM micrographs of carbon aerogels show wrinkled and
11 disordered GO-like sheets. The TEM results indicate good dispersion of GO in the
12 polybenzoxazine matrix and pores have been observed in the nanometer scale. The DSC results
13 indicated that addition of GO decreases the polymerization temperature of the SLTB(4HBA-
14 t403). Compared to the neat polybenzoxazine aerogel, the nanocomposite aerogels show better
15 thermal stability. The 50% weight loss temperature (T_{d50}) for aerogel and composite aerogels
16 containing 3, 5, and 10 wt% GO are 498, 527, and 605 °C, respectively, while T_{d50} for neat
17 polybenzoxazine aerogel is 396 °C. In addition, the char yield increased non-linearly with
18 increasing GO content, showing synergism. Hybridization of benzoxazine aerogels with GO as
19 highly porous structure of nanofiller provides special thermal and morphological properties of a
20 new class of nanocomposite aerogels, which are expected to find various applications, such as in
21 adsorption, catalytic, and conductive applications.

22

23

1 **Supporting Information**

2 See supporting information (SI) for experimental details of synthesis and characterizations of GO
3 and SLTB(4HBA-t403), additional FT-IR spectra of SLTB(4HBA-t403)/GO-5% hybrid aerogel.

4 This material is available free of charge via the Internet at <http://pubs.rsc.org>.

5

6 **ACKNOWLEDGMENTS**

7 The Ministry of Education of Libya is acknowledged for the financial support in the form of a
8 national scholarship to Almahdi Alhwaige. The authors thank Prof. Dr. Schiraldi at
9 Macromolecular Science and Engineering, Case Western Reserve University for his kind
10 support.

11

12 **REFRENCES**

- 13 [1] S. S. Kistler, *Phys. Chem.* 1932, **36**(1), 52-54.
14 [2] C. Tan, B. M. Fung, J. K. Newman, and C. Vu, *Adv. Mater.* 2001, **13**, 644-646.
15 [3] J. R. Johnson III, J. Spikowski, and D. A. Schiraldi, *ACS Appl. Mater. Interfaces* 2009, **1**,
16 1305-1309.
17 [4] S. M. Alhassan, S. Qutubuddin, and D. Schiraldi, *Langmuir* 2010, **26**, 12198-12202.
18 [5] A. I. Cooper and A. B. Holmes, *Adv. Mater.* 1999, **11**, 1270-1274.
19 [6] P. Lorjai, S. Wongkasemjit, T. Chaisuwan, and A. M. Jamieson, *Polym. Degrad. Stab.* 2011,
20 **96**, 708-718.
21 [7] H. Ishida, in *Handbook of Benzoxazine Resins*, H. Ishida and T. Agag, Eds., Elsevier,
22 Amsterdam 2011, 3-81.
23 [8] T. Takeichi, R. Zeidam, and T. Agag, *Polymer* 2002, **43**, 45-53.

- 1 [9] B. Kiskan, N. N. Ghosh, and Y. Yagci, *Polym. Int.* 2011, **60**, 167-177.
- 2 [10] N. N. Ghosh, B. Kiskan, and Y. Yagci, *Prog. Polym. Sci.* 2007, **32**, 1344-1391.
- 3 [11] Y. H. Wang, C. M. Chang, and Y. L. Liu, *Polymer* 2012, **53**, 106-112.
- 4 [12] F. W. Holly and A. C. Cope, *J. Am. Chem. Soc.* 1944, **66**, 1875-1879.
- 5 [13] X. Ning and H. Ishida, *J. Polym. Sci. Part A: Polym. Chem.* 1994, **32**, 1121-1129.
- 6 [14] A. Chernykh, J. Liu, and H. Ishida, *Polymer* 2006, **47**, 7664-7669.
- 7 [15] P. Lorjai, T. Chaisuwan, and S. Wongkasemjit, *J. Sol-Gel Sci. Technol.* 2009, **52**, 56-64.
- 8 [16] P. Katanyoota, T. Chaisuwan, A. Wongchaisuwat, and S. Wongkasemjit, *Mater. Sci. Eng.*
9 *B*, 2010, **167**, 36-42.
- 10 [17] U. Thubsuang, H. Ishida, S. Wongkasemjit, and T. Chaisuwan, *Microporous and*
11 *Mesoporous Mater.*, 2012, **156**, 7-15.
- 12 [18] T. Chaisuwan, T. Komalwanich, S. Luangsukrerk, and S. Wongkasemjit, *Desalination*,
13 2010, **256**, 108-114.
- 14 [19] K. Pakkethati, A. Boonmalert, T. Chaisuwan, and S. Wongkasemjit, *Desalination* 2011,
15 **267**, 73-81.
- 16 [20] D. A. Rubenstein, H. B. Lu, S. S. Mahadik, and W. *J. Biomater. Sci., Polym. Ed.* 2012, **23**,
17 1171-1184.
- 18 [21] Q. C. Ran, Q. Tian, C. Li, and Y. Gu, *Polym. Adv. Technol.* 2010, **21**, 170-176.
- 19 [22] N. Bitinis, M. Hernandez, R. Verdejo, J. M. Kenny, and M. A. -M. Lopez, *Adv. Mater.*
20 2011, **23**, 5229-5236.
- 21 [23] S. R. Hostler, A. R. Abramson, M. D. Gawryla, S. A. Bandi, and D. A. Schiraldi, *Int. J.*
22 *Heat Mass Transfer* 2009, **52**, 665-669.
- 23 [24] X. Fu and S. Qutubuddin, *Polymer* 2001, **42**, 807-813.

- 1 [25] P. Meneghetti, and S. Qutubuddin, *Thermochimica Acta*. 2006, **442**, 74-77.
- 2 [26] X. Chang, D. Chen, and X. Jiao, *J. Phys. Chem. B*. 2008, **112**, 7721-7725.
- 3 [27] M. Darder, P. Aranda, and E. -H. Ruiz, *Adv. Mater.* 2007, **19**, 1309-1319.
- 4 [28] K. -K. Ho, M. -C. Hsiao, T. -Y. Chou, C. -C. M. Ma,; X. -F. Xie, J. -C. Chiang, S. -H. Yang,
5 and L. -H Chang, *Polym. Intern.* 2013, **62**, 966-973.
- 6 [29] M. Zeng, J. Wang, R. Li, J. Liu, W. Chen, Q. Xu, and Y. Gu, *Polymer* 2013, **54**, 3107-
7 3116.
- 8 [30] S. M. Alhassan, S. Qutubuddin, D. A. Schiraldi, T. Agag, and H. Ishida, *Eur. Poly. J.* 2013,
9 **49**, 3825-3833.
- 10 [31] J. Potts, D. R. Dreyer, C. W. Bielawski, and R. S. Ruoff, *Polymer* 2011, **52**, 5-25.
- 11 [32] N. A. Kumar, H. -J. Choi, Y. R. Shin, D. W. Chang, L. Dai, and J. -B. Baek, *ACS
12 Nano*, 2012, **6**, 1715-1723.
- 13 [33] J. Shen, Y. Hu, C. Li, C. Qin, and M. Ye, *Small* 2009, **5**, 82-85.
- 14 [34] S. Stankovich, D. A. Dikin, R. D. Piner, K. A. Kohlhaas, K. Kleinhammes, Y. Jia, Y. Wu, S.
15 B. T. Nguyen, and R. S. Ruoff, *Carbon* 2007, **45**, 1558-1568.
- 16 [35] M. Seredych, A. V. Tamashausky, and T. J. Bandosz, *Adv. Funct. Mater.* 2010, **20**, 1670-
17 1679.
- 18 [36] D. A. Dikin, S. Stankovick, E. J. Zimney, R. D. Piner, G. H. B. Dommett, G. Evmenenko, S.
19 T. Nguyen, and R. S. Ruoff, *Nature* 2007, **448**, 457-460.
- 20 [37] F. Kim, J. L. Cote, and J. Huang, *Adv. Mater.* 2010, **22**, 1954-1958.
- 21 [38] Y. Xue, Y. Liu, F. Lu, J. Qu, H. Chen, and L. Dai, *J. Phys. Chem. Lett.* 2012, **3**, 1607-1612.
- 22 [39] A. Satti, P. Larpen, and Y. Gun'ko, *Carbon* 2010, **48**, 3376-3381.
- 23 [40] X. Zhao, Q. Zhang, and D. Chen, *Macromolecules* 2010, **43**, 2357-2363.

- 1 [41] M. A. Rafiee, J. Rafiee, Z. Wang, H. Song, Z. Z. Yu, and N. Korathar, *ACS Nano* 2009, **3**,
2 3884-3890.
- 3 [42] J. Wang and M. W. Ellsworth, *US Patent*, **2010**, 0144904, A1.
- 4 [43] X. Zhang, Z. Sui, B. Xu, S. Yue, Y. Luo, W. Zhan, and B. Liu, *J. Matar. Chem.* 2011, **21**,
5 6494-6497.
- 6 [44] A. A. Alhwaige, H. Ishida, T. Agag, and S. Qutubuddin, *RSC Adv.* 2013, **3**, 16011-16020.
- 7 [45] N. Zhang, H. Qiu, Y. Si, W. Wang, and J. Gao, *Carbon* 2011, **49**, 827-837.
- 8 [46] A. A. Alhwaige, Novel Biobased Chitosan/Polybenzoxazine Cross-Linked Polymers and
9 Advanced Carbon Aerogels for CO₂ Adsorption. **2014**, Ph.D. Thesis, Case Western
10 Reserve University, Cleveland, OH, USA.
- 11 [47] F. Tuinstra and J. L. Koenig, *J. Chem. Phys.* 1970, **53**, 1126.
- 12 [48] T. C. Chieu, M. S. Dresselhaus, and M. Endo, *Phys. Rev.* 1982, **26**, 5867.
- 13 [49] H. Ishida, and D. Allen, *Polymer* 1996, **37**, 4487-4495.
- 14 [50] C. Jubsilp, K. Punson, T. Takeichi, and S. Rimdusit, *Polym. Degrad. Stab.* 2010, **95**, 918-
15 924.
- 16 [51] H. Ishida, and Y. Rodriguez, *J. Appl. Polym. Sci.* 1995, **58**, 1751-1760.
- 17 [52] M. E. Smith, and H. Ishida, *Macromolecules* 1994, **27**, 2701-2707.
- 18 [53] A. Tuzun, B. Kiskan, N. Alemdar, A. T. Erciyes, and Y. Yagci, *J. Polym. Sci. Part A:*
19 *Polym. Chem.* 2010, **48**, 4279-4284.
- 20 [54] C. Jubsilp, B. Ramsiri, and S. Rimdusit, *Polym. Eng. Sci.* 2012, **52**, 1640-1684.
- 21 [55] J. Zhou, Z. Yao, Y. Chen, D. Wei, Y. Wu, and T. Xu, *Polymer Composites* 2013, **34**, 1245-
22 1249.
- 23 [56] Q. C. Ran, and Y. Gu, *J. Polym. Sci. Part A: Polym. Chem.* 2011, **49**, 1671-1677.

- 1 [57] A. A. Alhwaige, H. Ishida, and S. Qutubuddin, polybenzoxazine-based aerogels for
2 CO₂ adsorption, in preparation.
- 3 [58] Y. -C. Su, S. -W. Kuo, D. -R. Yei, H. Xu, and F. -C. Chang, *Polymer* 2003, **44**, 2187–
4 2191
- 5 [59] Y. -C. Yen, C. -C. Cheng, Y. -L. Chu and F. -C. Chang, *Polym. Chem.*, 2011, **2**, 1648–
6 1653
- 7 [60] A. A. Alhwaige, T. Agag, H. Ishida, and S. Qutubuddin, *Biomacromolecules* 2013, **14**,
8 1806-1815.
- 9 [61] B. Adhikari, A. Biswas, and A. Banerjee, *Appl. Mater. Interfaces* 2012, **4**, 5472-5482.
- 10 [62] V. C. Tung, J. kim, L. J. Cote, J. Huang, *J. Am. Chem. Soc.* 2011, **133**, 9262-9265.
- 11 [63] Y. Zhao, H. Ding, and Q. Zhong, *Appl. Surf. Sci.* 2012, **258**, 4301-4307.
- 12 [64] C. Pevida, T. C. Drage, and C. E. Snape, *Carbon* 2008, **46**, 1464-1474.
- 13 [65] I. Zafiropoulou, M. S. Katsiotis, N. Boukos, M. A. Karakassides, S. Stephen, V. Tzitzios,
14 M. Fardis, R. V. Vladea, S. M. Alhassan, and G. Papavassiliou, *J. Phys. Chem. C* 2013,
15 117, 10135-10142.
- 16 [66] L. Yang, C. Zhang, S. Pilla, and S. Gong, *Composites Part A*. 2008, **39**, 1653-1659.
- 17 [67] J. Dunkers and H. Ishida, *J. Polym. Sci. Part A. Polym. Chem.* 1999, **37**, 1913-1921.
- 18 [68] H. C. Schniepp, J. L. Li, M. J. Mcallister, H. Sai, M. H. Alonso, D. H. Adamson, R. K.
19 Prud'homme, R. Car, D. A. Saville, and I. A. Aksay, *J. Phys. Chem. B: Lett.* 2006, **110**,
20 8535-8539.